Quantum excitations of static charges in the Ginzburg-Landau model of superconductivity

Jeff Greensite and Kazue Matsuyama

Physics and Astronomy Department, San Francisco State University, San Francisco, California 94132, USA

We point out that in superconductors there may exist localized quantum excitations of the electric and condensate fields surrounding a static charge, which cannot be interpreted as simply the ground state of the screened charge plus some number of massive photons. This is illustrated via a lattice Monte Carlo calculation of the energy spectrum of a pair of separated static charges in an effective Ginzburg-Landau model of superconductivity.

I. INTRODUCTION

Composite quantum systems typically have a discrete spectrum of excitations, and although certain objects such as electrons and muons are referred to as "elementary" particles, this terminology can be a little misleading since in any interacting quantum field theory these elementary particles are inevitably surrounded by a field of some kind. In this sense, elementary particles are also composite. The question we would like to address here is whether there can exist a discrete spectrum of localized excitations in the fields surrounding a static charge and, in particular, whether this might be the case for the fields surrounding static ions in a superconductor.

In the condensed matter context, a screened ion in either the normal or superconducting phase, whether static or not, may be viewed as a type of quasiparticle. Of course, there is a ground state of the static charge surrounded by conduction electrons, but there is every reason to expect that such a many-body system would have a spectrum of quantum excitations above the ground state. Indeed, something of this sort accounts for the asymmetric line shape in x-ray photoelectron spectroscopy (XPS) spectra of metals in the normal phase [1], as we note later on. Our concentration here will be on the superconducting phase. If static ions in that phase have a discrete spectrum, distinct from that found in the normal phase, then the excited states of static ions in a superconductor are a new type of collective excitation, to be added to the list of such excitations in solids. We would expect that the existence of such states might manifest itself in the XPS spectra of metals in the superconducting phase.

Let us begin with the simplest case: a static charge coupled to the free quantized Maxwell field. Gauge invariance of physical states under infinitesimal gauge transformations, embodied in the Gauss Law, insists that the static charge must be the source of an electric field. The ground state of the static charge + gauge field system, as shown long ago by Dirac [2], is given by

$$|\Psi_{\boldsymbol{x}}\rangle = \overline{\psi}(\boldsymbol{x})\rho(\boldsymbol{x};A)|\Psi_0\rangle, \qquad (1)$$

where $\overline{\psi}(\boldsymbol{x})$, operating on the vacuum, creates the static charge and

$$\rho(\boldsymbol{x};A) = \exp\left[-i\frac{e}{4\pi}\int d^3z\, A_i(\boldsymbol{z})\frac{\partial}{\partial z_i}\frac{1}{|\boldsymbol{x}-\boldsymbol{z}|}\right]. \qquad (2)$$

In the state $|\Psi_{\boldsymbol{x}}\rangle$, the expectation value of the electric field is simply the Coulomb field of the static charge. The operator $\rho(x;A)$, which depends only on the gauge field, is an example of what we call a "pseudomatter" operator.[1] Operators of this kind, functionals of only the gauge field, transform under an infinitesimal gauge transformation like a static charge, but are invariant under global gauge transformations $g(x) = g$ in the center of the gauge group, which in this case is $g(x) = \exp(i\theta) \in$ global U(1). As a result, the physical state (1) is not *entirely* gauge invariant; in fact, it transforms covariantly under such global U(1) transformations, i.e.,

$$|\Psi_{\boldsymbol{x}}\rangle \rightarrow e^{-i\theta}|\Psi_{\boldsymbol{x}}\rangle. \qquad (3)$$

This is characteristic of an isolated charge in electrodynamics, unscreened by any matter fields. It should be emphasized that covariance under the global U(1) subgroup of the gauge group is in no way a violation of the physical state condition (i.e., the Gauss law), which does not require invariance under global transformations that affect neither the gauge field nor the charge densities. Of course, this global symmetry of the action may or may not be a symmetry of the vacuum. As we have discussed extensively elsewhere [3], it is the global center subgroup of the gauge group which is broken spontaneously in the Higgs phase of a gauge Higgs theory, with a corresponding gauge-invariant order parameter closely analogous to the Edwards-Anderson order parameter [4] for a spin glass.

---

[1]It is worth noting that $\rho^*(x;A)$ is also the gauge transformation to a Coulomb gauge. In fact, if $g(x;A)$ is the gauge transformation to a physical gauge defined by some condition $F[A] = 0$ imposed on each time slice, then it is not hard to see that $g^*(x;A)$ is the pseudomatter operator. This statement can be readily generalized to non-Abelian theories.

Symmetry breaking of this kind is not a violation of Elitzur's theorem, which forbids the spontaneous breaking of local, rather than global symmetries. While the transition to the Higgs phase is not necessarily a thermodynamic transition, it is nonetheless accompanied by a change in physical behavior, which is either the loss of metastable flux tube states and Regge trajectories (transition from the confinement phase) or the disappearance of massless vector bosons (transition from the Coulomb phase).

For our purposes, the free-field example is not so interesting. Of course, there are excitations of the charge+quantized field combination, but these excitations consist simply of some number of photons, of arbitrary positive energies, superimposed on a background Coulombic field; they are not the localized excitations with a discrete energy spectrum that are of interest here. We therefore move on to gauge Higgs theories, including those which, like the Ginzburg-Landau model, may simply be the effective theory of some more fundamental physics in which the Higgs field is composite. There is already evidence of excitations of static charges in SU(3) gauge Higgs theory [5] and in the Abelian Higgs model [6]. But the theories of phenomenological interest would be the Ginzburg-Landau model of superconductivity and the electroweak sector of the standard model. A spectrum of quark and lepton excitations or, more precisely, a spectrum of localized excitations of the fields surrounding quarks and leptons would obviously be of great interest, but here we face the formidable complication that the electroweak theory is a chiral gauge theory, which resists a lattice formulation.[2] For that reason, we turn our attention to quantum behavior in the Ginzburg-Landau model with static ions.

II. THE CALCULATION

The effective Ginzburg-Landau action is (cf. [8])

$$S = \int d^4x \left\{ \frac{1}{2} \rho_s \left[\frac{1}{v^2} (\partial_0 \xi + 2eA_0)^2 - (\nabla \xi - 2e\mathbf{A})^2 \right] + \frac{1}{2} (E^2 - B^2) \right\}, \tag{4}$$

where ξ is the Goldstone mode, $\rho_s = n_s/2M$ where n_s, M, $2e$ are the Cooper pair density, mass, and charge, respectively, and $v \sim 10^{-2}$ is of the order of the ratio of the Fermi velocity in a metal to the speed of light. The mass of the transverse photon in the continuum formulation is, in natural units,

$$M_{ph} = \frac{1}{\lambda_L} = 2e\sqrt{\rho_s}, \tag{5}$$

where λ_L is the London penetration depth. The transition to the lattice formulation in Euclidean time, which is the non-relativistic version of the charge $q = 2$ lattice Abelian Higgs

model, is straightforward:

$$S_{\text{eff}} = -\beta \sum_{\text{plaq}} \text{Re}[UUU^*U^*]$$

$$- \gamma \sum_x \sum_{k=1}^{3} \text{Re}[\phi^*(x)U_k^2(x)\phi(x+\hat{k})]$$

$$- \frac{\gamma}{v^2} \sum_x \text{Re}[\phi^*(x)U_0^2(x)\phi(x+\hat{t}), \tag{6}$$

where $\beta = 1/e^2 \approx 10.9$, $\phi = e^{i\xi}$, $\rho_s = \gamma/a^2$, and a is the lattice spacing. A choice of gamma, together with an observed London penetration depth and the tree-level relationship (5), requires a lattice spacing

$$a = 2e\gamma^{\frac{1}{2}}\lambda_L. \tag{7}$$

Obviously, the continuum limit would require $\gamma \to 0$, but this is impossible because of a transition to the massless phase at finite γ. At $\beta = 10.9$, we find, from investigation of the susceptibility of $\langle \text{Re}[\phi^*(x)U_k^2(x)\phi(x+\hat{k})]\rangle$, a transition close to $\gamma = 0.017$ (see the Appendix). So it must be emphasized that the lattice formulation is an effective theory, valid beyond some inherent short distance cutoff which, since Cooper pairs are composite, would most naturally be the diameter of a Cooper pair. In most texts, this effective theory is treated classically, but here we would like to treat the effective theory as a quantum theory in its own right, with a short distance cutoff a. In lattice Monte Carlo simulations of S_{eff}, it is convenient to fix to the unitary gauge, in which case, since $1/v^2 \sim 10^4$, it is a very good approximation to take $U_0(x) = \pm 1$.

The aim is to search for excitations around pairs of widely separated static $q = \pm 1$ (e) charges, having fixed ions in mind. We are obliged to consider pairs of charges for technical reasons discussed below, which are related to the fact that one cannot create a single charge in a periodic volume. We therefore consider physical states of the following form:

$$|\Phi_n(\mathbf{x}, \mathbf{y})\rangle = Q_n(\mathbf{x}, \mathbf{y})|\Psi_0\rangle, \tag{8}$$

with

$$Q_{2n-1}(\mathbf{x}, \mathbf{y}) = \overline{\psi}(\mathbf{x})\zeta_n(\mathbf{x})\zeta_n^*(\mathbf{y})\psi(\mathbf{y}),$$

$$Q_{2n}(\mathbf{x}, \mathbf{y}) = \overline{\psi}(\mathbf{x})\phi(\mathbf{x})\zeta_n^*(\mathbf{x})\zeta_n(\mathbf{y})\phi^*(\mathbf{y})\psi(\mathbf{y}), \tag{9}$$

where $\overline{\psi}$, ψ are static fermion operators, and the pseudomatter operators $\zeta_n(\mathbf{x})$ are eigenstates of the covariant Laplacian operator,

$$\sum_{\mathbf{y}} (-D^2)_{\mathbf{x}\mathbf{y}}\zeta_n(\mathbf{y}) = \lambda_n \zeta(\mathbf{x}), \tag{10}$$

where

$$(-D^2)_{\mathbf{x}\mathbf{y}} = \sum_{k=1}^{3} [2\delta_{\mathbf{x}\mathbf{y}} - U_k(\mathbf{x})\delta_{\mathbf{y},\mathbf{x}+\hat{k}} - U_k^\dagger(\mathbf{x}-\hat{k})\delta_{\mathbf{y},\mathbf{x}-\hat{k}}]. \tag{11}$$

Note that $\zeta_n(\mathbf{x})$ is a pseudomatter operator, and $\phi(\mathbf{x})\zeta_n^*(\mathbf{x})$ transforms like a pseudomatter operator. We have found it important, in the calculations discussed below, to include both.

Now let us consider a subspace of Hilbert space spanned by N physical states $\{|\Phi_n(\mathbf{x}, \mathbf{y})\rangle, n = 1, \ldots, N\}$, and let τ be

---

[2]See, however, the attempt to find excitations in a chiral U(1) theory in [7].

the transfer matrix. Define the rescaled transfer matrix,

$$\mathcal{T} = \tau e^{\mathcal{E}_0}, \tag{12}$$

where $\mathcal{E}_0$ is the vacuum energy [or, more precisely, if κ_0 is the largest eigenvalue of τ, then $\mathcal{E}_0 = -\ln(\kappa_0)$]. We would like to construct a set of eigenstates of $\mathcal{T}$ in the truncated basis. For this nonorthogonal basis, we first calculate numerically the matrix elements and overlaps,

$$[\mathcal{T}]_{\alpha\beta}(R) = \langle\Phi_\alpha|\mathcal{T}|\Phi_\beta\rangle = \langle Q_\alpha^\dagger(\boldsymbol{x}, \boldsymbol{y}, 1)Q_\beta(\boldsymbol{x}, \boldsymbol{y}, 0)\rangle,$$

$$[O]_{\alpha\beta}(R) = \langle\Phi_\alpha|\Phi_\beta\rangle = \langle Q_\alpha^\dagger(\boldsymbol{x}, \boldsymbol{y}, 0)Q_\beta(\boldsymbol{x}, \boldsymbol{y}, 0)\rangle, \tag{13}$$

where $R = |\boldsymbol{x} - \boldsymbol{y}|$, and $Q(\boldsymbol{x}, \boldsymbol{y}, t)$, in Euclidean time path-integral formulation, is the $Q(\boldsymbol{x}, \boldsymbol{y})$ operator acting at time t. We obtain the eigenvalues of $\mathcal{T}$ in the subspace by solving the generalized eigenvalue problem,

$$[\mathcal{T}]\boldsymbol{v}^{(n)} = \lambda_n[O]\boldsymbol{v}^{(n)}, \quad |\Psi_n(\boldsymbol{x}, \boldsymbol{y})\rangle = \sum_{\alpha=1}^{N} v_\alpha^{(n)}|\Phi_\alpha(\boldsymbol{x}, \boldsymbol{y})\rangle. \tag{14}$$

Each $|\Psi_n(\boldsymbol{x}, \boldsymbol{y})\rangle$ is a linear combination of the nonorthogonal basis states $|\Phi_\alpha(\boldsymbol{x}, \boldsymbol{y})\rangle$, and the set of states $\{|\Psi_n(\boldsymbol{x}, \boldsymbol{y})\rangle\}$ are the energy eigenstates (i.e., eigenstates of the transfer matrix) of the isolated static pair in the subspace.

Let us define, for M pseudomatter operators ζ_α, the $N = 2M$ operators,

$$V_{2\alpha-1}(\boldsymbol{x}, \boldsymbol{y}, U) = \zeta_\alpha(\boldsymbol{x})\zeta_\alpha^*(\boldsymbol{y}),$$

$$V_{2\alpha}(\boldsymbol{x}, \boldsymbol{y}, U) = \zeta_\alpha^*(\boldsymbol{x})\phi(\boldsymbol{x})\phi^*(\boldsymbol{y})\zeta_\alpha(\boldsymbol{y}). \tag{15}$$

In order to calculate the required matrix elements numerically, we integrate out the heavy fermions (via a hopping parameter expansion [9]) to obtain

$$[\mathcal{T}^T]_{\alpha\beta}(R) = \langle\Phi_\alpha|\mathcal{T}^T|\Phi_\beta\rangle$$

$$= \langle Q_\alpha^\dagger(\boldsymbol{x}, \boldsymbol{y}, T)Q_\beta(\boldsymbol{x}, \boldsymbol{y}, 0)\rangle$$

$$= \langle V_\alpha^\dagger[\boldsymbol{x}, \boldsymbol{y}; U(t+T)]P^\dagger(\boldsymbol{x}, t, T)$$

$$\times V_\beta[\boldsymbol{x}, \boldsymbol{y}; U(t)]P(\boldsymbol{y}, t, T)\rangle$$

$$[O]_{\alpha\beta}(R) = \langle V_\alpha^\dagger[\boldsymbol{x}, \boldsymbol{y}; U(t)]V_\beta[\boldsymbol{x}, \boldsymbol{y}; U(t)]\rangle, \tag{16}$$

where indices α, β range from 1 to N, and

$$P(\boldsymbol{x}, t, T) = U_0(\boldsymbol{x}, t)U_0(\boldsymbol{x}, t+1)\cdots U_0(\boldsymbol{x}, t+T-1) \tag{17}$$

is a timelike Wilson line of length T. In (16), we have dropped powers of the fermion mass in the hopping parameter expansion, which only contribute an overall constant to the energy of the fermion-antifermion system, and are therefore irrelevant to the question of excitations.

The eigenstates $\{|\Psi_n\rangle\}$ of the transfer matrix in the N-dimensional subspace are in general not eigenstates of the transfer matrix in the full Hilbert space. But it may happen that Ψ_1, the state with the lowest energy expectation value in the subspace, has a very large overlap with the static charge ground state in the full Hilbert space, and it follows that the $\Psi_{n>1}$ would have a correspondingly small overlap. On general

grounds,

$$\mathcal{T}_{nn}(R, T) \equiv \langle\Psi_n|\mathcal{T}^T|\Psi_n\rangle$$

$$= \sum_{\alpha\beta} v_\alpha^{*(n)}\langle Q_\alpha^\dagger(\boldsymbol{x}, \boldsymbol{y}, T)Q_\beta(\boldsymbol{x}, \boldsymbol{y}, 0)\rangle v_\beta^{(n)}$$

$$= \sum_k |c_k(R)|^2 e^{-E_k(R)T}, \tag{18}$$

where E_k is the energy above the ground state of the kth energy eigenstate in the full Hilbert space, containing a static fermion-antifermion pair separated by a distance R. If $\Psi_{n>1}(\boldsymbol{x}, \boldsymbol{y})$ has a large overlap with one excited energy eigenstate Ψ_i^{exact} and a very small overlap with the ground state, then we may expect that for some range of $T_{\min} \leqslant T \leqslant T_{\max}$,

$$\mathcal{T}_{nn}(R, T) \approx |c_i(R)|^2 e^{-E_i(R)T}, \quad T_{\min} \leqslant T \leqslant T_{\max}, \tag{19}$$

and in that case we may extract the excitation energy $E_i(R)$ from a logarithmic plot of $\mathcal{T}_{nn}(R, T)$ vs T.

Of course, there is no guarantee that a strategy of this kind will work. It relies on the conjecture that the overlap of $|\Psi_1\rangle$ with the true $\overline{\psi}\psi$ ground state is very large. Even if this conjecture is true, it might be the case that the excited states are simply the ground state plus one or more gauge bosons, as in pure QED. But the general idea is testable, and our results for the Ginzburg-Landau model in the Higgs phase are reported in the next section.

A. Why not single fermion states?

Before presenting numerical results, we would like to address this question: why not consider single fermion states of the form

$$\Omega_\alpha = \overline{\psi}(\boldsymbol{x})\zeta_\alpha(\boldsymbol{x})\Psi_0, \tag{20}$$

where ζ_α is a pseudomatter field. We assume that there is some algorithm which determines $\zeta(\boldsymbol{x}, t)$ uniquely on time slice t from the spacelike link variables on that time slice. Such numerical algorithms exist for Laplacian eigenstates, and also for numerical fixing to the Coulomb gauge.[3] The latter determines the gauge transformation to the Coulomb gauge, which is itself a pseudomatter field, in a finite periodic volume.

Now consider the transfer matrix elements,

$$\langle\Omega_\alpha|\mathcal{T}|\Omega_\beta\rangle = \langle\zeta_\alpha^\dagger(\boldsymbol{x}, 1)U_0^\dagger(\boldsymbol{x}, 0)\zeta_\beta(\boldsymbol{x}, 0)\rangle, \tag{21}$$

which is essential to our discussion of energy expectation values. The problem here is that the operator on the right-hand side of (21) is not invariant under gauge transformations $g(\boldsymbol{x}, t) = e^{i\theta(t)}$ or, in an SU(N) gauge theory, under transformations $g(\boldsymbol{x}, t) = z(t) \in Z_N$. Transformations of this kind do not alter spacelike links, and hence do not alter the pseudomatter fields $\zeta_\alpha(\boldsymbol{x})$. Nor do these transformations, which in each time slice belong to the global Z_N center subgroup of the gauge group, alter the gauge-invariant action. But they *do* transform the timelike links $U_0(\boldsymbol{x}, t)$. As a result, the matrix

---

[3]The iterative gauge-fixing algorithms used in computer simulations are deterministic and fix to a unique Gribov copy satisfying the gauge-fixing condition.

elements (21) all vanish, at least in a finite periodic volume. This is very general, i.e., it holds both in pure gauge theory and gauge Higgs theories, and it is one way of understanding why, on the lattice, it is impossible to place a single charge in a periodic volume, despite the fact that one can numerically transform the gauge field to some unique Gribov copy of the Coulomb gauge. If there were a single-charged matter field in the theory, call it φ, then the same objection would not hold for the neutral state,

$$\Psi = \overline{\psi}(\boldsymbol{x})\varphi(\boldsymbol{x})\Psi_0, \qquad (22)$$

as the operator $\overline{\psi}(\boldsymbol{x})\varphi(\boldsymbol{x})$ is fully gauge invariant, including under global gauge transformations, and the expression in (21), with ζ replaced by φ, is invariant under $g(\boldsymbol{x}, t) = e^{i\theta(t)}$. But there are no such single-charged dynamical fields in the Ginzburg-Landau model under consideration.

It is for these reasons that we must consider pseudomatter states with two static charges,

$$\Phi_{\alpha\beta}(\boldsymbol{x}, \boldsymbol{y}) = \overline{\psi}(\boldsymbol{x})\zeta_\alpha(\boldsymbol{x})\zeta_\beta^*(\boldsymbol{y})\psi(\boldsymbol{y})\Psi_0, \qquad (23)$$

where the ζ_α are eigenstates of the covariant Laplacian operator. But here there is still an ambiguity, in that if $\zeta_\alpha(\boldsymbol{x})$ is a Laplacian eigenstate, then so is

$$\zeta_\alpha'(\boldsymbol{x}; U) = e^{iF_\alpha[U]}\zeta_\alpha(\boldsymbol{x}; U), \qquad (24)$$

where $F_\alpha[U]$ is any real-valued functional of the link variables. So, in general, we may expect that any $\zeta_\alpha(\boldsymbol{x}; U)$ determined by the Arnoldi algorithm will have wild fluctuations in a global phase factor as U is varied, and fluctuations of that sort will cause

$$\langle\Phi_{\alpha\beta}|\mathcal{T}^T|\Phi_{\alpha\beta}\rangle \qquad (25)$$

to vanish, for any $T > 0$, and $\alpha \neq \beta$. And, in fact, this is what is observed in numerical simulations. For this reason, we must restrict our considerations to states Φ_n of the form (8) and (9), where there is no remaining ambiguity, and any global phase factor as in (24) cancels out.

B. Photon mass

The photon mass in the Ginzburg-Landau model is determined from the time correlation of space-averaged gauge-invariant link operators. We define

$$G(t) = \frac{1}{3}\sum_{i=1}^{3}\langle\mathcal{A}_i(t)\mathcal{A}_i(0)\rangle, \qquad (26)$$

where

$$\mathcal{A}_i(t) = \frac{1}{L^3}\sum_{\boldsymbol{x}}\text{Im}[\phi^\dagger(\boldsymbol{x}, t)U_i^2(\boldsymbol{x}, t)\phi(\boldsymbol{x} + \hat{i})]. \qquad (27)$$

Now, on very general grounds, $G(t)$ is related to a spectrum of excitations with quantum numbers of the photon as follows:

$$G(t) = \lim_{T\to\infty}\frac{1}{3}\sum_{i=1}^{3}\frac{\langle 0|e^{-H(T-t)}\mathcal{A}_i(t)e^{-Ht}\mathcal{A}_i(0)e^{-HT}|0\rangle}{\langle 0|e^{-2HT}|0\rangle}$$

$$= \sum_n\left(\frac{1}{3}\sum_{i=1}^{3}|\langle 0|\mathcal{A}_i|n\rangle|^2\right)e^{-(\mathcal{E}_n-\mathcal{E}_0)t}$$
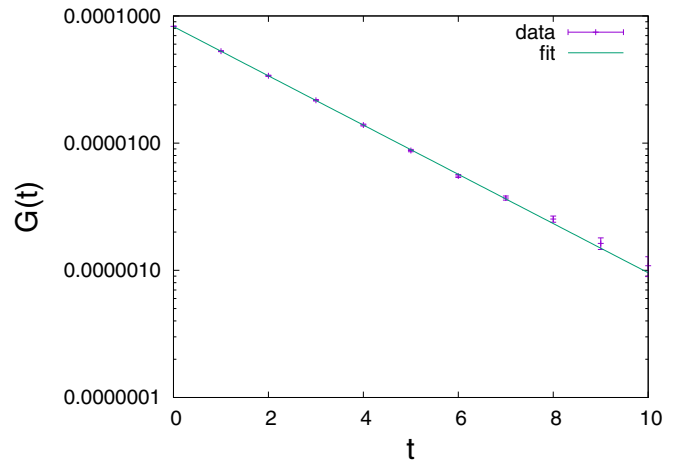
$$= \sum_n a_n e^{-E_n t}, \qquad (28)$$

FIG. 1. Determination of the photon mass at $\beta = 10.9$, $\gamma = 0.6$ from the time correlator $G(t)$ of space-averaged gauge-invariant link variables $\mathcal{A}_i$ on a $16^3 \times 36$ lattice volume. The straight line on the logarithmic plot is a best fit of $ae^{-m_{ph}t}$ to the data, where m_{ph} is the photon mass and a is a constant.

where the $\mathcal{E}_n$ are energy eigenvalues, and $E_n = \mathcal{E}_n - \mathcal{E}_0$ are energies above the vacuum energy of states $|n\rangle$ with the quantum numbers of $\mathcal{A}_i$. For large t, the sum is dominated by the lowest energy state, i.e., the state containing a single massive photon at rest, and therefore

$$m_{ph} = -\lim_{t\to\infty}\frac{d}{dt}\ln G(t). \qquad (29)$$

In practice, in a finite range where $G(T)$ fits a straight line on a logarithmic plot, the data for $G(t)$ are fit by a single exponential,

$$G(t) \approx ae^{-m_{ph}t}, \qquad (30)$$

in that range, and from the best fit we can extract the photon mass m_{ph}.

A typical result, at $\beta = 10.9$ and $\gamma = 0.60$, is shown in Fig. 1. The data were taken on a $16^3 \times 36$ lattice volume, with 400 lattices separated by 100 sweeps. The data are fit very precisely, in the range $1 \leqslant t \leqslant 10$, by a single exponential; evidently the contribution of higher excitations is negligible in this correlator. Then, m_{ph} is extracted from a best fit of a single exponential (30) to the $G(t)$ data, from which we derive a value of $m_{ph} = 0.446(3)$ for the photon mass in lattice units. The accuracy of the straight line fit indicates that the contribution of more energetic states to the sum in (28) is negligible. A similar fit with the same parameters, except for $\gamma = 0.25$, results in $m_{ph} = 0.288(1)$. We note that both of these values are quite close to the tree-level expression $m_{ph} = 2e\sqrt{\gamma}$ (with m_{ph} in lattice units), obtained by multiplying both sides of Eq. (5) (where M_{ph} is in physical units) by the lattice spacing a.

III. EXCITATIONS

We set $\beta = 10.9$, corresponding to $e^2/4\pi = 1/137$ in natural units, and begin with Higgs coupling $\gamma = 0.6$ on a $12^3 \times 36$ lattice volume. We consider static charge $q = \pm 1$ pairs at all pairs of lattice coordinates $\boldsymbol{x} = (x_1, x_2, x_3)$, $\boldsymbol{y} = (y_1, y_2, y_3)$
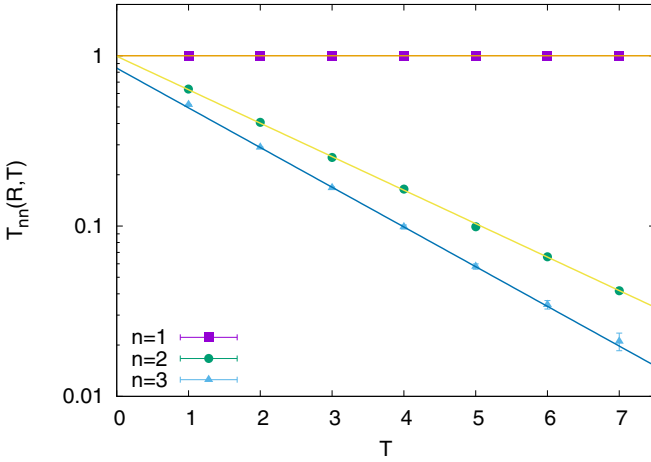
FIG. 2. $\mathcal{T}_{nn}(R, T)$ vs T at $R = 5.83$, for $n = 1, 2, 3$, together with their best fits. The corresponding energies $E_n(R)$ are extracted from the slope of exponential fits on a logarithmic plot. This data were obtained on a $12^3 \times 36$ lattice volume at $\beta = 10.9$ and $\gamma = 0.60$.
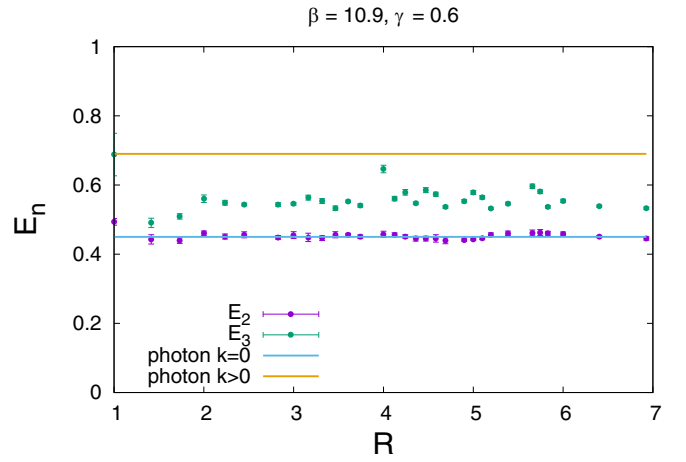

FIG. 3. Energies $E_n(R)$ vs R for $n = 2, 3$ again at $\gamma = 0.60$ on a $12^3 \times 36$ lattice volume. The lower solid line represents the mass of a massive photon, and the upper line is the energy of a massive photon at the lowest possible momentum on this finite periodic lattice.

with $y_i = x_i + \Delta_i$ and $-4 \leqslant \Delta_i \leqslant 4$. This allows a maximum off-axis separation of $R = |\boldsymbol{x} - \boldsymbol{y}| = 6.93$. Four Laplacian eigenstates $\zeta_n(\boldsymbol{x})$, and therefore eight operators $Q_\alpha(R)$ at each R, were used in the computation.

Figure 2 shows an example of our results for $\mathcal{T}_{nn}(R, T)$ at $R = 5.83$. We see that $\mathcal{T}_{11}(R, T) = 1$, independent of T, to a very high degree of precision. This means that the ground-state energy is $E_1(R) = 0$, and it turns out that this result is obtained at all R, not just at $R = 5.83$. The $\mathcal{T}_{22}$ and $\mathcal{T}_{33}$ data are fit to an exponential,

$$c_n(e^{-E_n T} + e^{-E_n(36-T)}). \tag{31}$$

It can be seen that the data for $\mathcal{T}_{22}$, $\mathcal{T}_{33}$ fall off linearly on the logarithmic plot, with fits taken in the range [2,7], and the slopes are slightly different, corresponding to a small energy difference between E_2 and E_3. Beyond $T = 8$ or so, there are rather large error bars, so those points are not included in the fit.

The energies $E_2(R)$, $E_3(R)$ vs R are displayed in Fig. 3. Also shown is the mass of a static photon (blue line) at $\gamma = 0.6$, as obtained in the previous section, along with the energy of the massive photon $\sqrt{m_{ph}^2 + (2\pi/12)^2}$ at the minimal nonzero momentum on a periodic lattice of length 12. The ground-state energy, not shown here, is at $E_1(R) = 0$.

The energy $E_2(R)$ of the first excited state above the ground state pretty nearly coincides with the photon mass. So this state is easy to interpret: it is simply the ground state of the static charges plus a static photon. The second excited state, of energy $E_3(R)$, cannot be interpreted in that way because (with the possible exception of one outlier) it lies above the one-photon mass, but below the energy of a photon with minimal momentum in a 12^3 space volume. So there are two possibilities. One is that this state represents the energy of a static photon plus a small excitation, of energy $\Delta E = E_3 - m_{ph}$, of the field surrounding the static charge pair. But, in that case, we might expect to see this energy ΔE as the energy of the first excited state, i.e., an excitation without the massive photon, which is not seen. The second possibility is that E_3

represents an excitation energy of the static charges with no extra photons, which happens to lie above the threshold for photon production, and this seems more likely. It, of course, implies that in the infinite volume limit, where the photon momentum can take on any value, this excitation is metastable and could decay via massive photon emission. On the other hand, if the charges are very far apart, this option might be strongly suppressed since the excitation energy of the field surrounding either charge is only half the total excitation energy, $\frac{1}{2}E_3$.

From the data, it appears that $\Psi_1(\boldsymbol{x}, \boldsymbol{y})$ and $\Psi_2(\boldsymbol{x}, \boldsymbol{y})$ are very close to the true ground state, and the ground state plus a massive photon, respectively. We note in passing that this result required use of both types of operators shown in (9). Use of only the Q_{2n-1} operators results in data that are not easily fit by a single exponential.

A. Other Higgs couplings, volumes, and excitations

There is no visible dependence on R in $E_1(R)$, and very little in $E_2(R)$ in Fig. 3. However, we see significant scatter in the values shown for $E_3(R)$, which cannot be attributed to error bars in the exponential fit. We conjecture that the reason for this scatter is that $|\Psi_3(\boldsymbol{x}, \boldsymbol{y})\rangle$, while close to the true energy eigenstate, may contain enough (probably random) admixtures of higher excited states to show a rather small, mainly random dependence on R.

This ties into the question of finite volume effects. In Fig. 4, we display in separate subfigures our data for the E_2, E_3, E_4 excitation energies vs R, for $12^3 \times 36$, $16^3 \times 36$, and $20^3 \times 36$ lattice volumes. There are two points to note. First, the fluctuations in $E_n(R)$ with R increase with n, but clearly decrease at larger volumes. Second, there is a slight tendency in the data for $E_n(R)$ to decrease at larger volumes. However, we see that this lowering in $E_3(R)$, while noticeable in going from a $12^3 \times 36$ to a $16^3 \times 36$ volume, is almost negligible going from $16^3 \times 36$ to a $20^3 \times 36$ volume, particularly at larger R. A convincing demonstration that the E_3 data have converged on the $20^3 \times 36$ volume would really require extrapolation of
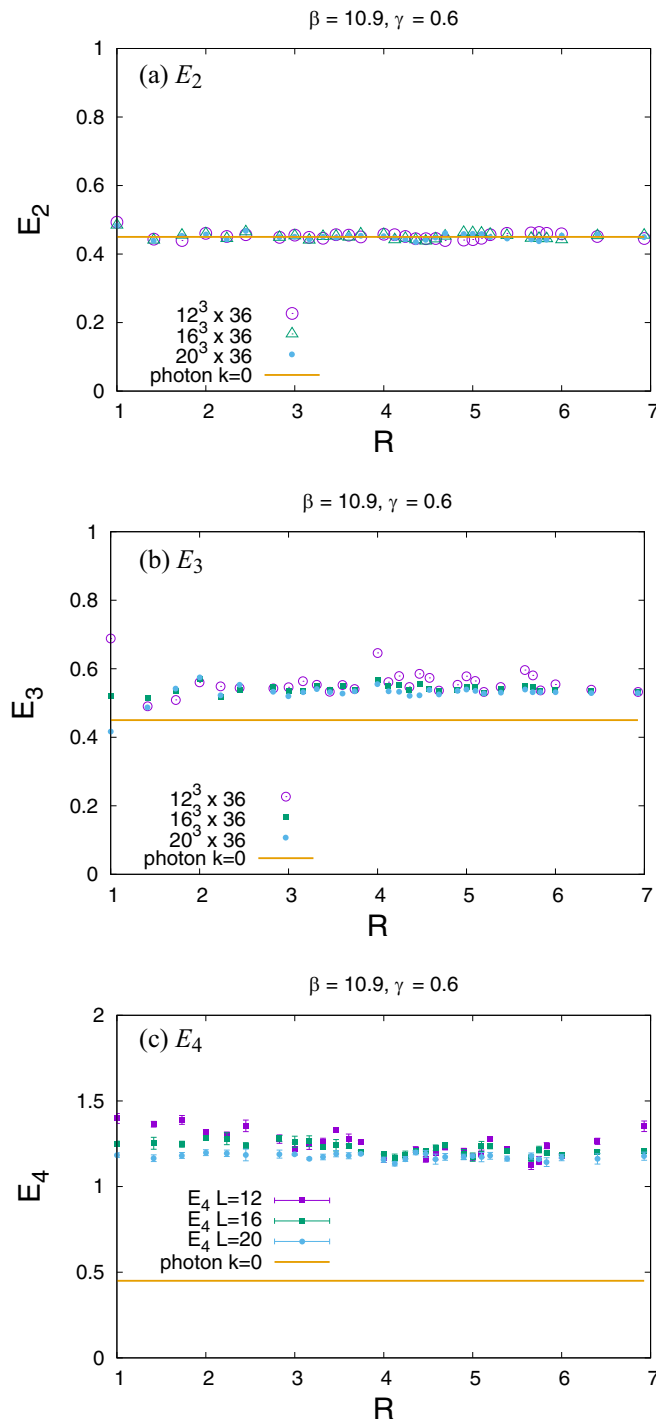
FIG. 5. Energies $E_{2,3,4}(R)$, but this time at $\gamma = 0.25$, with $\beta = 10.9$ and lattice volume $16^3 \times 36$. The lower and upper solid lines represent the energies of a static massive photon, and a photon of minimal momentum for this periodic volume.

FIG. 4. Excitation energies $E_n(R)$ vs R for lattice volumes 12^3, 16^3, $20^3 \times 36$. (a) $E_2(R)$, (b) $E_3(R)$, (c) $E_4(R)$. Note that fluctuations with R tend to decrease with higher volumes.

the data to infinite volume, and this in turn would call for computation on a very large range of volumes, which seems impractical at this stage. So we must keep in mind that there may yet be some reduction in the values of $E_3(R)$ at still larger volumes, although we doubt, from the data seen in Fig. 4(b), that this could be very substantial.

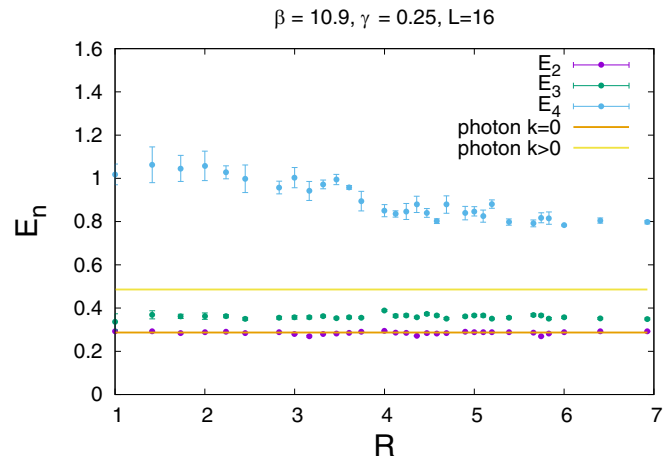At spatial extension $L = 16$, the energy of a photon with smallest nonvanishing momentum is at $E = 0.597$, which is

very close to the E_3 data points. If we had only the data on the $16^3 \times 36$ volume, we would probably conclude that E_3 corresponds to the ground state plus a massive photon of that kind. But this interpretation is inconsistent with the data found on the smaller $12^3 \times 36$ volume, and since increasing the volume has only a minimal effect on the values of E_3, we conclude that we are seeing the same state in both volumes, i.e., an excitation above the ground state of the static ions, rather than a photon of nonzero momentum. The data for E_4 likewise vary only a little from the $16^3 \times 36$ to the $20^3 \times 36$ volume, which argues against an interpretation involving one or more photons of finite momentum.

Figure 5 shows the results of the same calculation of E_{2-4} on a $16^3 \times 36$ volume, with the same exponential fit in the range $T \in [2, 7]$, but this time with $\gamma = 0.25$. The mass of the massive photon is, of course, reduced (in lattice units) as γ is reduced, as one expects, but the results are similar. The next question is: how similar are the results?

B. Scaling

We have computed the photon mass and excitations E_n in lattice units for two different γ values, namely, $\gamma = 0.25, 0.60$. For a given London penetration depth λ_L, we can compute the lattice spacing and from there convert the charge separation R, photon mass, and excitation energies in physical units. Let $m_{ph}(\gamma)$ be the photon mass in lattice units found at a particular γ value, and $M_{ph}(\gamma) = m_{ph}(\gamma)/a$ be the corresponding photon mass in physical units, where a is the lattice spacing given in Eq. (7). We then have

$$\frac{M_{ph}(\gamma_1)}{M_{ph}(\gamma_2)} = \sqrt{\frac{\gamma_2}{\gamma_1}} \frac{m_{ph}(\gamma_1)}{m_{ph}(\gamma_2)}. \tag{32}$$

Inserting the computed values of $m_{ph}(\gamma = 0.25) = 0.288(1)$ and $m_{ph}(\gamma = 0.60) = 0.446(3)$ in lattice units, we find the ratio of photon masses in physical units to be

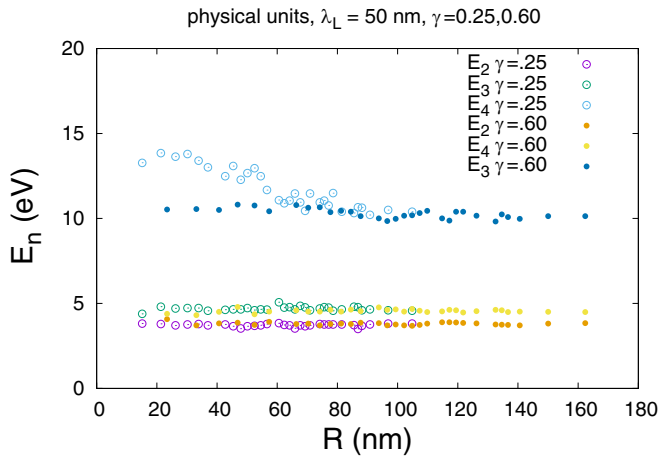$$\frac{M_{ph}(0.25)}{M_{ph}(0.60)} = 1.000(8). \tag{33}$$

FIG. 6. A test of scaling. Using a fixed London penetration depth of $\lambda_L = 50$ nm to set the scale, we convert both R and $E_{2,3,4}(R)$ to physical units at both $\gamma = 0.25$ and $\gamma = 0.60$, with $\beta = 10.9$ fixed.

If we choose a typical London penetration depth, say $\lambda_L = 50$ nm, we can compare data for E_n vs R in physical units, obtained at the two γ values. The result, for data taken on a $16^3 \times 36$ lattice volume, is shown in Fig. 6. E_1 is consistent with zero for both γ values, and the excitations E_2, E_3 essentially coincide. Values for E_4 differ at small R, but appear to converge at larger R. The overall conclusion is that the results in physical units do not really depend on γ, at least at larger charge separations.

IV. DISCUSSION

The Ginzburg-Landau model is, of course a simplified effective theory of superconductivity, presumably relevant at scales beyond the diameter of a Cooper pair. But if the Ginzburg-Landau model is not misleading us, then the results presented here do suggest a possible experimental test via x-ray photoelectron spectroscopy (XPS).

We have argued that the self-interacting field surrounding a static charge may have a spectrum of localized excitations. In a certain sense, this has already been seen in normal metals. The electric field of a static charge which is suddenly inserted into a normal metal is, of course, screened by electrons in the conduction band, and one can ask whether these screening electrons themselves have a spectrum of excitations. The answer appears to be yes, and this is the origin of the asymmetric line shape in the core electron XPS spectrum, as pointed out long ago by Doniach and Sunjic [1] (for a simplified discussion, cf. [10]). When an electron is ejected from the valence band, this corresponds to a sudden appearance of an isolated charge in the metal, and the process of screening can leave the charge plus Fermi sea in one of a near continuum of excitations slightly above the screened ground state since very little energy is required to create electron-hole excitations near the Fermi level. This results in the Doniach-Sunjic line shape, which closely fits the XPS data.

According to our results in the Ginzburg-Landau model, things may be a little different in the XPS spectrum of core electron emission in the superconducting phase of a conventional superconductor. We have found a discrete spectrum of

TABLE I. Comparison of $E_{2,3,4}(R)$ at $\beta = 10.9$ and $\gamma = 0.25, 0.60$ at $R = 5.83$, obtained from fitting the corresponding $\mathcal{T}_{nn}(R, T)$ vs T data in the different fitting intervals shown.

Fitting interval	$E_2^{0.6}$	$E_3^{0.6}$	$E_4^{0.6}$	$E_2^{0.25}$	$E_3^{0.25}$	$E_4^{0.25}$
2–4	0.472	0.543	1.18	0.288	0.363	0.83
2–5	0.472	0.540	1.13	0.286	0.357	0.81
2–6	0.453	0.538	1.13	0.282	0.354	0.81
2–7	0.453	0.537	1.13	0.282	0.353	0.82
2–8	0.453	0.537	1.13	0.282	0.350	0.81

excitations of the condensate, with energies of the order of mass of the massive photon. This mass, which in natural units is the inverse of the London penetration depth, depends on the metal, but in general is of the order of a few electron volts. So in the superconducting phase, we would expect to see a number of additional peaks in the core electron emission spectrum, separated from the main peaks by a few ev. Unfortunately, the experimental situation is a little different from our idealized setup of two static charges. One of the charges, namely, the hole left by the emitted core electron, is indeed static, and we would expect the condensate distribution around the hole to be no different from the idealized situation. The emitted electron, however, is by no means static, which complicates making a precise prediction for the location of the additional peaks. If this complication is ignored, then given the Landau penetration depth λ_L, the positions of those peaks are calculable. For, e.g., $\lambda_L = 50$ nm, the excitation energies for widely separated charges are the E_3, E_4 energies seen in Fig. 6 at the larger separations. The relative heights and widths of these extra peaks depend on microscopic dynamics determining transition amplitudes and lifetimes, which are beyond the scope of the simplified effective model.

It appears that a comparison of XPS core electron spectra above and below the superconducting transition, for conventional (or, for that matter, high T_c) superconductors, has not yet been done. At least, we have not been able to find a comparison of this type in the literature. An experimental investigation along these lines could, for present purposes, be very helpful.

An obvious question is whether quarks and leptons in the electroweak sector of the standard model, which is also a gauge Higgs theory, would have a spectrum of excitations analogous to what we find in the Ginzburg-Landau model. If so, these would appear as "elementary" particles in their own right. Unfortunately, in the absence of a lattice formulation of chiral gauge theory having a positive transfer matrix and a sensible continuum limit, we are unable to make any predictions. Should such a formulation ever become available, it would be possible to compute an excitation spectrum along the lines presented here.
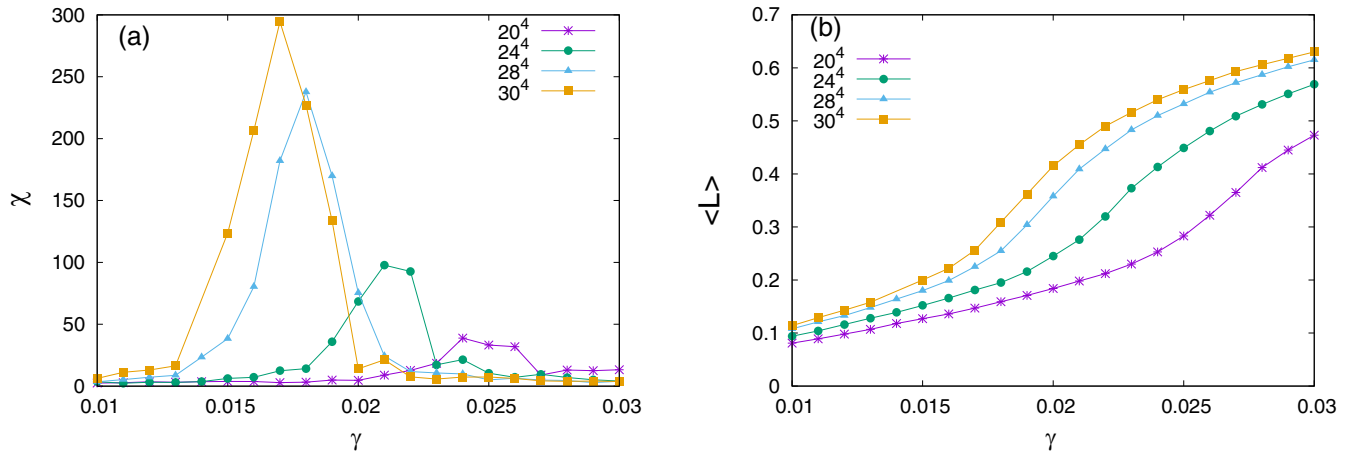
FIG. 7. (a) Link susceptibility χ vs γ and (b) gauge-invariant link $\langle L \rangle$ vs γ, on a variety of lattice volumes.

APPENDIX: NUMERICAL DETAILS

In all cases we have constructed, on each time slice, the Laplacian eigenstates ζ_n with the four lowest eigenvalues, leading to eight $|\Psi_n\rangle$ states, according to the procedures described above. The Laplacian eigenstates were computed numerically via the Arnoldi algorithm, as implemented in the ARPACK software package [11]. Data for $[\mathcal{T}^T]_{\alpha\beta}(R)$, along with error bars for those values, were obtained by averaging the results of 10 independent Monte Carlo simulations at $\gamma = 0.25, 0.60$ on $12^3 \times 36$, $16^3 \times 36$ and (at $\gamma = 0.60$) $20^3 \times 36$ lattice volumes. In each simulation, 120 lattice configurations were generated after 5000 thermalizing sweeps, with data taking sweeps separated by 100 Monte Carlo update sweeps. The numerical solution of the generalized eigenvalue problem was carried out by the MATLAB eig routine, which derived values and error bars for $\mathcal{T}_{nn}(R, T)$. The determination of $\{E_n\}$ from fits to a single exponential, and the corresponding error bars, were obtained from the GNUPLOT software [12].

Fitting data points over a finite range raises the question of what is the "best" range and how the answers would differ if the range were slightly modified. Although the lattice was large enough in the time direction to compute $\mathcal{T}_{nn}(R, T)$ up to $T = 18$, in practice we found the statistical errors were significant for data points beyond $T = 8$. Excluding points beyond those limits and dropping the first data point (which would be the most susceptible to mixing from higher excitations), we can compare the values for $E_{2,3,4}$ using slightly different fitting intervals. Typical results are shown in Table I, for

$R = 5.83$, and lattice size $16^3 \times 36$, where $E_n^{0.25}, E_n^{0.60}$ refer to excitation energies computed at $\gamma = 0.25$ and $\gamma = 0.60$, respectively. Error bars for E_2, E_3 were approximately 1%, and 3–4% for E_4, which, given the small dependence on R, could indicate a slight overestimate of error bars on the fitted data points. The excitation energies shown in our figures were derived for a fitting interval of R in the range 2–7, but it is clear that choosing a different interval would not affect our conclusions.

As mentioned in the text, at $\beta = 10.9$ we located a phase transition, presumably to the massless phase, at the rather low γ value of $\gamma \approx 0.017$. This was determined from inspection of the link susceptibility,

$$\chi = V(\langle L^2 \rangle - \langle L \rangle^2), \qquad (A1)$$

where V is the lattice volume and

$$L = \frac{1}{3V} \sum_x \sum_{k=1}^{3} \mathrm{Re}[\phi^*(x) U_k^2(x) \phi(x + \hat{k})], \qquad (A2)$$

with the result shown in Fig. 7(a). At each volume, data were taken on 1400 lattices separated by 100 sweeps, after 20 000 thermalizing sweeps. In previous work on the relativistic Abelian Higgs model, we have seen that the transition to the massless phase corresponds to a discontinuity (a "kink") in the slope of L in the infinite volume limit (cf. Fig. 1 in [13]). Although this is not as obvious in our Ginzburg-Landau data, there is some evidence of such a kink developing, as the volume increases, in Fig. 7(b).

[1] S. Doniach and M. Sunjic, J. Phys. C **3**, 285 (1970).

[2] P. A. M. Dirac, Can. J. Phys. **33**, 650 (1955).

[3] J. Greensite and K. Matsuyama, Phys. Rev. D **101**, 054508 (2020); Symmetry **14**, 177 (2022).

[4] S. F. Edwards and P. W. Anderson, J. Phys. F **5**, 965 (1975).

[5] J. Greensite, Phys. Rev. D **102**, 054504 (2020).

[6] K. Matsuyama, Phys. Rev. D **103**, 074508 (2021).

[7] J. Greensite, Phys. Rev. D **104**, 034508 (2021).

[8] P. Coleman, *Introduction to Many-Body Physics* (Cambridge University Press, Cambridge, 2015).

[9] C. Gattringer and C. B. Lang, Lect. Notes Phys. **788**, 1 (2010).

[10] S. Hüfner, *Photoelectron Spectroscopy: Principles and Applications*, Advanced Texts in Physics (Springer, Berlin, 2013).

[11] See https://www.caam.rice.edu/software/ARPACK/.

[12] See www.gnuplot.info.

[13] K. Matsuyama and J. Greensite, Phys. Rev. B **100**, 184513 (2019).